Testing concrete E-modulus at very early ages through several techniques: an inter-laboratory comparison

Brice Delsaute[1], Claude Boulay[2], José Granja[3], Jérôme Carette[1], Miguel Azenha[3], Cédric Dumoulin[1], Grigorios Karaiskos[1], Arnaud Deraemaeker[1], Stéphanie Staquet[1]

[1] ULB – Université Libre de Bruxelles
BATir Department
Brussels
Belgium
Tel: +32 2 650 27 58; Fax: +32 2 650 27 82
sstaquet@ulb.ac.be, corresponding author

[2] IFSTTAR – Institut Français des Sciences et Technologies des Transports, de l'Aménagement et des Réseaux
Materials and Structures Department
Paris-East University
Paris
France
Tel: +33 2 38 31 21 88; Fax: +33 1 81 66 89 81

[3] ISISE – Institute for Sustainability and Innovation in Structural Engineering
University of Minho, School of Engineering
Department of Civil Engineering
Campus de Azurém
4800-058 Guimarães
Portugal
Tel: +351 253 510 200; Fax: +351 253 510 217

ABSTRACT
The design of concrete structures is based on calculation rules, which often do not take into account the very early age behaviour of the material. However, during this period, structural concrete is subjected to strains due to the hydration process of cement. If these strains are restrained by concrete itself or surrounding boundaries, stresses start to build up that can lead to the formation of cracks. Among the parameters involved in the stress build up, the stiffness evolution is of major importance. This paper reports the use of eight different techniques aimed at stiffness evolution assessment, applied on the same concrete mix, in a round robin experimental test within three laboratories. The observations are compared after having expressed the results at the same equivalent age. Both the loading stress rate and amplitude are observed to have an effect of limited importance on the determination of the quasi-static elastic modulus, which might be explained by very short term creep. Ultrasonic measurements provide values of E-modulus that are higher than the values provided by the quasi static tests at the time of the concrete setting. Similar mechanisms associated to very short term creep could explain the difference between the quasi-static and high-frequency elastic modulus.

KEYWORDS
Early age behaviour of concrete; Young's modulus; Round robin test; High-frequency; Ultrasonic measurements.

1 INTRODUCTION

Concrete is a composite material that undergoes major mechanical properties changes during its curing process. Thus for a good structural design, it becomes extremely important to know the concrete structural behaviour from the beginning of the hardening process. However, design rules are not yet well adapted to the real behaviour of concrete for the period between the setting time, or t_0, and approximately one day. Before t_0, good practices for making, casting and curing of concrete allow avoiding cracking of fresh concrete [1, 2]. After t_0, physico-chemical strains can develop. Upon restraint (i.e. by rebars, formworks, already cast concrete), these volume changes can be the cause for surface or traversing cracks. Obviously, permeability, service life and aesthetic of structures are affected by these cracks. A lack of attention to this early age period at the stages of design, experimental assessment or in practice can lead to major defects. For example, Aïtcin *et al.* [3] describes a value of "forgotten" strain between t_0 and one day in the case of an autogenous shrinkage measurement on a high performance concrete. Indeed, they report that the autogenous shrinkage between t_0 and 1 day is equal to 250x10^{-6} m/m whereas its development between 1 and 3 days solely amounts to 50x10^{-6} m/m. For a concrete, this difference can explain the appearance of cracks or not. Another important issue is the experimental determination of the setting time of concrete. This point was already been addressed in the work of Weiss [4] and Sant *et al.* [5]. In these articles, the opportunity to use a parameter or another to monitor the concrete setting (thermal, chemical, electrical, mechanical parameters) is discussed.

In this paper, similar or complementary methods are compared within three laboratories working on the same concrete. As stresses are induced by restrained volume changes, the E-modulus evolution of concrete since the earliest age is of major importance, not only for the determination of the setting time but also for modelling and numerical computation purposes. That is why three laboratories involved in the work reported herein, researches have been focused on experimental methods leading to a better assessment of mechanical properties. This is a timely and opportune research work, as no recent inter-technique and inter-laboratory comparisons have been found in the literature except the preliminary work done by the authors in [6], in concern to concrete E-modulus at early ages. Eight different techniques have been implemented in the three laboratories. They can, a priori, be sorted in three classes, according to their respective ranges of loading rates. There are four techniques of quasi-static loadings (**QS_0**: classical extensometry (all three labs); **QS_1**: automated loading with BTJASPE (IFSTTAR), **QS_2**: automated loading using QS_1 protocol (IFSTTAR), **QS_3**: automated loading with a TSTM (ULB)); one technique of resonant frequency loadings (**RF**: EMM-ARM testing technique (UMinho)) and three techniques of high frequency loadings (**HF_1**: classical UPV measurements with FreshCon (ULB), **HF_2**: classical UPV measurements with BTPULS (IFSTTAR) , **HF_3**: smart aggregates (ULB)). These different protocols were applied without necessarily controlling the temperature history of the specimens in the same way, often due to practical limitations associated to the test setups and the size of specimens themselves. That is why observations are compared after having expressed results at the same concrete maturity using the equivalent time method [7]. These techniques scan a wide variety of ways for monitoring the E-modulus of concrete since the earliest age. They are suitable for both industrial and research applications. In the following lines, the specimen preparation and the concrete characterization will be presented first. Then, each of the eight testing methods (**QS_0, QS_1, QS_2, QS_3, RF, HF_1, HF_2, HF_3**) will be described into details. Finally, it will be followed by the analysis of the results organized in three parts: firstly, a comparison between the results obtained with the low frequency testing methods (**QS_1, QS_2, QS_3, RF**) with a discussion on the effect of the stress amplitude and the stress-rate on the results obtained with the low frequency testing methods; secondly, a discussion on the results obtained with the high frequency testing methods only (**HF_1, HF_2, HF_3**) and thirdly, a discussion on the relation between the results obtained with the low frequency testing methods and the high frequency testing methods.

2 SPECIMEN PREPARATION AND MATERIAL CHARACTERIZATION

The same material is used in the three laboratories. The mixture proportions are given in Table 1. Fresh concrete was mixed mechanically or manually depending on the volume of the batch (from 2 litres to approx. 40 litres). Even though these differences can lead to scattered results, no significant effect was observed in the performed experiments on this concrete as presented in section 4.1.4.

The strength evolution was useful for quantifying the limits of the automatic loadings (tests presented in sections 2.1.3 and 2.1.4) applied at early age in order to avoid any damage of the samples. The samples were cylinders (Ø 110 mm x 220 mm) or cubes (100 mm). They were cured inside adhesive aluminium tape at 20 ºC, and capped with sulphur mortar when necessary. Results are reported on Figure 1.

For the sake of these calculations, the compressive strength is modelled by the following model:

$$f_{cm} = a \cdot e^{-\frac{c}{t}} - b \qquad \textbf{(1)}$$

With: $f_{cm}(t)$ expressed in MPa

a = 38.04 MPa, b = 1.67MPa, c = 24 hours

t: equivalent time since mixing (in hours)

The activation energy was determined through calorimetric testing. This parameter, associated to temperature recordings, allowed calculations, based on Arrhenius laws, of an equivalent age (t_{eq}) [8, 9,10] for each of our results. These calculations were performed at a fixed reference temperature equal to 20 °C.

The setting period corresponds to a period between the time when a needle penetrates completely a sample of mortar or cement grout and the time when it does not penetrate anymore the sample [5, 11, 12]. In field applications, the final setting time has also been identified, as mentioned by Sant *et al.* [5], like the time when the bleeding water is reabsorbed which indicates the creation of vapour spaces in the matrix. As penetration tests do not apply specifically for concrete, the work of Robeyst *et al.* [13] compared ultrasonic testing to penetration tests performed on sieved concrete by removing the coarse aggregates. They used ultrasonic P-waves in transmission mode. The evolution of the ultrasonic pulse velocity shows an experimental S shape and the corresponding derivative function is calculated. The final setting was considered to occur when the value of this derivative function decreases down to 80 % of the peak value. This last technique was applied in the present research work. It is worth underlining that the final setting corresponds to a time when a sample can be manipulated, but gently to avoid any rupture. Before this time, any manipulation leads to a rupture. It is also the time when the stiffness of the material begins to increase significantly. This final setting is, here, called t_0 [14]. An estimation of this time is required for starting tests just after concrete setting.

Measurements of the modulus of elasticity were performed in the 3 laboratories and stress rates were ranging from 0.20 to 0.55 MPa/s for the three laboratories (see Table 2 and Table 3). Table 4 shows the results of the mean values of the quasi-static loading E modulus obtained by the three laboratories according to the reference test set up (QS_0) presented in section 3.1.1.

As loading protocols are very similar, these results are mixed in order to obtain a single description of the evolution of the E-modulus by these classical means as it is shown in Figure 2.
For the sake of the analysis of our results, the following mathematical model is proposed (Figure 2):

$$E(t) = d - e.\left(\frac{\tau}{t}\right)^{f} \tag{2}$$

Where $E(t)$ is expressed in GPa,
t: equivalent time since mixing (in hours),
d = 41.57 GPa, e = 191.04 GPa, $\boldsymbol{\tau}$= 1 h and f = 0.72.

This mathematical model has been calibrated to fit the quasi-static loading E-modulus results obtained with the reference set up (QS_0) and shown in Table 4. This model is used in Figures 2, 13, 14, 16, 17, 25 and 27 as a reference curve for comparison.
This equation was already used in [15] to model the growth of bacteria populations but it has been chosen only for its mathematical properties for the determination of the early age properties of cement based material.

This function is accepted as the reference for the comparisons between the different methods and will thus be used recurrently in the following sections.

This kind of test does not provide an accurate estimation of t_0; as the first measurement could only be made 1h and 40 minutes after a t_0 determined by other means (UPV, QS_1 or RF) presented in section 3.1; 3.2 and 3.3.

3 DESCRIPTION OF THE METHODS

3.1 Quasi-static loadings

3.1.1 Reference tests (QS_0)

In the three laboratories, the reference tests (QS_0) were performed, after the concrete setting (t_0), on cylinders at different ages. For each test, strains were measured by extensometers. For the three laboratories, the extensometers are almost similar: i.e. three transducers (LVDTs) measuring the relative displacement between two rings fixed to the specimen, as presented on Figure 3. Prior to the test, specimens were kept in a curing chamber at 20ºC. However, the protocol of loading, size of the specimen and extensometers used for the E-modulus determination presented some differences among the three involved laboratories, as synthesized in Table 2 which follows the nomenclature of Figure 3. The selected testing ages associated to the results are given further in Table 4.

At IFSTTAR, the testing specimens were cylinders with 110 mm in diameter and 220 mm in length. The first tests were performed as early as 7 hours after casting. Strains were measured by extensometers, with results comparable to those of strain gauges [16]. The protocol of loading consisted in applying four cycles between 5 and 30 % of the strength measured on other cylinders (with the same geometry) just before the test [17]. The quasi-static E-modulus is evaluated during the loading cycle. The loading rate was set to 0.50 MPa/s. The testing equipment included a hydraulic actuator with 500 kN of maximum load.
At ULB, similar cylinders and the same extensometer were used. 20% of the concrete strength at the time of the test was applied within 10 seconds, on four different samples. Corresponding stress rates were ranging from 0.20 to 0.55 MPa/s, depending on the age of the sample. The quasi-static E-modulus is evaluated during the loading cycle. The testing equipment included a hydraulic actuator with 1000 kN of maximum load.
At the University of Minho, cylinder specimens (150 mm in diameter and 300 mm in length), have been tested under cyclic compression according to LNEC E397 [18]. The protocol of loading consisted in applying five cycles

between 0.80 MPa and 33 % of the ultimate strength at the age of testing. The quasi-static E-modulus is evaluated during the loading cycle. The loading rate was set to 0.30 MPa/s. The testing equipment included a hydraulic actuator with 2000 kN of maximum load.

3.1.2 Automated and quasi-static loading with BTJASPE (Béton Très Jeune Age Suivi de la Prise et du module d'Elasticité) or QS_1

BTJASPE (QS_1) is a recent device, developed at IFSTTAR [19, 20, 21,22]. It allows the automatic monitoring of the stiffness of a concrete cylinder remaining in its mould. Measurements start just after the concrete casting and continue up to a few days. The device is placed between the plates of an automatic testing machine. The temperature of the sample is kept at a constant value thanks to a circulation of water inside a double walled mould. The sample (Figure 4 #1) is 100 mm in diameter and 200 mm in length. The mould wall (#2), made of stainless steel, has a thickness of 1 mm. Its depth is 254 mm. Once the concrete has been placed, the loading is applied via a steel piston (#3) guided inside the upper part of the mould. Fixed to this piston, three arms (#4) support three LVDTs, placed at 120° around the mould. These transducers measure the mean longitudinal displacement. This measurement includes the length change of the sample and the length changes of the steel piston and of the base of the rig (#5).
An upper conical loading plate (#6) includes a system, composed of a moving tip whose position is measured by a LVDT sensor with a resolution of 0.65 µm. This measurement indicates to the testing machine, during the approach, the relative position between the upper platen and the piston (#3). When the contact is detected, a loading, controlled thanks to the measurement of the mean longitudinal displacement, is triggered. This protocol is effective even if the concrete is still in its fresh state. Then, the compressive loading of the sample is ensured at a constant strain rate (5µstrain/s). When a relative strain equal to 100 µstrains is reached, the ramp is reversed in order to unload the sample. This strain value is chosen to avoid any damage of the sample in compression. This protocol allows starting the tests shortly after the concrete casting. A new loading cycle is triggered after a delay of about 15 to 30 minutes. The device is placed on a lower plate (#7). It is surrounded by a cylindrical housing where a circulation of water allows removing the heat coming from the piston of the testing machine.
The quasi-static E-modulus is evaluated during the loading cycle. The main measurements (load vs mean longitudinal displacement) allow the calculation of an experimental resulting stiffness of the sample in series with the bearings of the device (K). The separation of these two parts is based on a relationship (2nd degree polynomial) giving the E-modulus of the concrete in function of the experimental stiffness, K:

$$E = g.K^2 + h.K \text{ with E in GPa, K in kN/mm, } g=1.03\ 10^{-5}\ kN^{-1} \text{ and } h= 0.0227\ mm^{-1} \qquad \textbf{(3)}$$

The coefficients of this polynomial have been fitted on the results obtained by a finite element calculation performed during the design of the device [19]. During this calculation increasing values of the numerical E-modulus of concrete were used to obtain the corresponding stiffness. It is assumed that, in the experimentation, the concrete sample remains in its elastic zone so that the experimental stiffness and the numerical stiffness are equal.
It can be underlined that the effect of the reinforcement due to the presence of the stainless steel mould has been stated, experimentally, as negligible. Indeed, prior to the casting, a thin layer of grease is applied on the inner wall of the mould. The Poisson's effect does not lead to a radial displacement exceeding the thickness of this layer of grease.

3.1.3 Automated quasi-static loading using QS_1 protocol (QS_2)

In order to check the accuracy of BTJASPE device and the degree of confinement in the stainless steel mould of the sample, tests using the same loading protocol were performed on concrete cylinders removed from their cardboard mould just after the concrete setting detected by UPV measurements. The sample, capped with a sulphur mortar, is equipped with three extensometers and placed between the upper and the lower platens used for QS_1 (Figure 5). A ball joint is placed between the upper face of the sample and the upper loading platen. In that case, the sample is not confined thus the results are not affected by any lateral effect excepted near the ends of the sample. These tests were used to validate the results obtained with QS_1 [19]. This test used the same type of extensometer as those of QS_0 and QS_2.

3.1.4 Automated quasi static loadings with a TSTM (QS3)

Since 2006, a Temperature Stress Testing Machine (TSTM) has been under development in ULB-BATir for testing concrete since t_0, under free and restraint conditions [20, 23, 24]. The testing machine is a Walter+Bay LFMZ 400 kN electromechanical testing setup. The machine is composed by a fixed steel head, a central unidimensional part and a moving end (Figure 6a). In the central part, where the measurements of the displacements are taken, the stress field is assumed to be homogenous (Figure 6b) and the section is equal to 100x 100 mm². The displacements are recorded by Foucault current's sensors (contact free sensors) having a resolution of 0.014 µm. Before casting, a plastic sheet is placed in the mould to ensure sealed conditions. Moreover, the plastic sheet helps also to reduce, with the presence of Teflon, the friction between the sample and the mould. The machine is equipped with a double walled mould allowing a thermal regulation and, in particular, ensuring isothermal curing conditions. Temperature measurements took place in the central part of the specimen and in each head. The experiment was conducted in a climatic chamber with temperature of 20±1ºC.

A new methodology was developed for the monitoring of the E-modulus. The test is controlled at a constant loading rate, thanks to the software DION® (Walter & Bai). The test begins shortly after t_0. For each cycle of loading, the moving end of the testing machine is controlled by the force sensor, up to 20% of the compressive strength at the age of testing. The sample is then unloaded until it reaches a null force. Recordings (displacements, force and temperature) are taken during the cycles and more specifically during each loading and unloading. These displacement measurements can then be directly used to compute the E-modulus. The quasi-static E-modulus is evaluated during the loading cycle. The duration between each loading was approximately 60 minutes. The relation between the stresses and the strains is quasi linear during the loading. In order to keep the strictly linear zone of the stress/strain curve, the E-modulus is calculated between 30 and 80% of the maximum load reached in each cycle.

3.2 Resonant frequency method (RF)

The EMM-ARM testing technique (Elasticity Modulus Measurement through Ambient Response Method) has been initially proposed by Azenha *et al.* [25] for the continuous measurement of concrete stiffness since the instant of casting. It is called here RF (Resonant frequency). Since its initial proposal for concrete testing, it has been extended towards application to cement paste [26], cement stabilized soil [27] and structural adhesives [28]. A more recent work has demonstrated the in situ applicability of the method and introduced changes that allow re-usability of parts [29]. The application of the RF method, in the context of this research, was fully made at the UMinho laboratory.

The general principle of RF consists on continuously monitoring the first flexural resonant frequency of a composite beam with known geometry and support conditions, which contains the material to be tested since the fresh state. The evolution of resonant frequency can be directly and quantitatively correlated to the evolution of E-modulus of the tested material, without any kind of ambiguity of user dependency. The test procedure is fully automated and provides results in real time.

For the experiments envisaged in this research, three testing geometries have been adopted, both based on simply supported conditions for the test beam: (i) the cylinder shaped specimen inside an acrylic mould (RF_A) (Figure 7); (*ii*) a similar cylindrical shape beam similar to the one presented in Figure 7 but with internal/external diameters of 84/90 mm and 900 mm of span, and made of PVC (RF_P); (*iii*) the prismatic shaped specimen inside a reusable metallic mould (RF_M) (Figure 8). Even though the experimental setups, and interpretation techniques have been thoroughly explained and discussed in previous publications [25, 27], some brief remarks are given here for the sake of self- sufficiency of this paper.

The acrylic mould (RF_A) is 2000 mm long, with internal/external diameter of 92/100 mm, density $\rho = 1286.89$ kg/m^3 and E-Modulus of $E_{acrylic} = 3.30$ GPa. The PVC mould (RF_P) is 1000 mm long, with internal/external diameter of 84/90mm, density of 1463.49 kg/m^3 and Young's Modulus of 4.50 GPa. Both moulds are crossed by horizontal rods at their supporting points (longitudinally spaced by 1800 mm and 900 mm for the beams RF_A and RF_P, respectively) and vertical rods that act as connectors of mould/specimen. Lids are utilized at the extremities: one fixed lid, placed before casting and a removable lid, aimed to be placed after casting. Due to the nature of the moulds, they require inclined/vertical position for casting. As soon as the removable lid is placed in position and excess air is purged, the composite beams are placed under simply supported conditions on the rods which are in turn placed on concrete blocks. At this stage, an accelerometer is attached to the mid span section of each of the beams (see Figure 7), and the test starts.

The metallic beam was devised for reusability and increased robustness for in situ application [29]. It is made of a 'U-shaped' metallic alloy plate ($\rho_{plate} = 7800$ kg/m^3 and $E_{plate} = 170$ GPa), that has a total length of 2600 mm. The space for concrete placement spans through the central 2400 mm of the mould, with a cross section of 150 x 150 mm². The cross section shape of the mould was devised to assure that the centre of gravity of the metallic beam coincides with the centre of gravity of the tested concrete. Lids are placed near the extremity of the beam, right over the place where steel supports are placed to assure a free span of 2.4 m. Two aluminium stiffeners exist at 800 mm from the supports, in order to avoid significant transverse deformations of the metallic plates due to the weight of concrete. Connectors are also placed at 200 and 700 mm from the supports, according to the cross sectional scheme shown in Figure 8, in order to assure full bond conditions. Three accelerometers are placed on the bottom surface of the beam according to the positions shown in Figure 8. This variant geometry of EMM-

ARM results in easier casting operations, as the mould is kept in its final testing position since the instant of casting, with the accelerometers placed in position even before casting, which was not possible with the acrylic/PVC moulds. Also, the reusability of the mould provides a more sustainable testing protocol, from both the economic and environmental points of view. The feasibility of the metallic mould for EMM-ARM has been tested and reported in a previous work [29] with satisfactory results. All mould beams are tested in the scope of this work to extend their mutual validation and make a deeper analysis of the relative adequacy of these methods to test very early stiffness developments of concrete.

Accelerations of the monitored points have been measured for 28 days with sampling frequency of 200 Hz and PCB accelerometers with 10 V/g sensitivity, 0.15 to 1000 Hz frequency range and 225 grams of mass. Packets of 60 seconds of data have been taken every 15 minutes with a 24 bit data logger (NI 9234). Data processing to obtain the resonant frequency of the beams was made through the Welch procedure [30], involving windowing, averaging and Fourier transforms, according to a process that has been described in detail in [25]. Based on the resonant frequency of the composite beams, and the detailed knowledge of their geometries, mould stiffness and global masses, the stiffness of the tested concrete was obtained through analytical derivations based on the dynamic equations of motion of the corresponding composite beam (detailed explanations in [25]). This procedure was implemented in LabVIEW [31], thus allowing continuous automatic information about the calculated E- modulus in all tested beams. Temperature measurements took place in the central point of the cross section of each concrete specimen. The experiment was conducted in a climatic chamber with temperature of 19.2 ± 0.5 ºC.
A final remark is given in regard to the applicability of the analytical derivation of the equations of motion used for E modulus estimation: before the structural setting instant, such equations that rely on several assumptions related to concrete as a solid material may not hold, and therefore the EMM-ARM E-modulus estimations before setting time shown in Figure 16 are plotted as dashed lines. In fact, even though the reported evolutions seem quite feasible, they may not be rigorous at this period.

3.3 Ultrasonic Pulse Velocity (UPV) measurements

3.3.1 Classical UPV measurements: HF_1 and HF_2

On this concrete, two classical techniques of ultrasonic measurements were performed [32, 33, 34]. First, the FreshCon (HF_1) device (see Figure 9) developed at the University of Stuttgart was used due to its ability to detect very early age signals. Ultrasonic pulses of 5 µs at 800 V are sent through ultrasonic transducers (0.5 MHz resonant frequency). The ultrasonic pulse velocity (UPV) can therefore be computed before setting. In addition, the UPV was measured with a BTPULS (Béton Transmission Par Ultra Sons, HF_2) device developed at IFSTTAR [20, 35]. This additional test, performed after the setting, was performed for comparative purposes between these two techniques.

For HF_1, the sample thickness is 47 mm, which is more than twice the size of the largest aggregate (44 mm). Two samples are cast inside two similar containers: one for P-waves measurements and one for S-waves measurements. Samples are placed in a thermally regulated chamber and their temperatures are measured continuously during the test. Detailed information about this method can be found in [34].
The P-waves (V_P) and S-waves (V_S) velocities can be used to compute the high frequency Poisson's ratio (ν_{HF}) and E modulus (E_{HF}) through equations 4 and 5, where ρ is the concrete density:

$$\nu_{HF} = \frac{1-2\cdot\left(V_S^2/V_P^2\right)}{2-2\cdot\left(V_S^2/V_P^2\right)} \tag{4}$$

$$E_{HF} = V_P^2\cdot\rho\cdot\frac{\left(1+\nu_{HF}\right)\cdot\left(1-2\cdot\nu_{HF}\right)}{\left(1-\nu_{HF}\right)} \tag{5}$$

These equations apply for a homogeneous and isotropic solid. When they are used during the hardening process of a concrete, it is assumed that these conditions are fulfilled as soon as the age is higher than t_0. Before this time, the UPV is highly affected by the presence of entrapped air inside the concrete [36]. Thus, even though very early age recordings are feasible, the relevance of the results remains controversial.
For HF_2 [37], the P-waves are emitted at the bottom and received at the top of a 110 mm diameter and 220 mm height cylinder in its cardboard mould (Figure 10). Up to three samples can be tested simultaneously.

3.3.2 *Smart aggregates (HF_3)*

The main drawback of the HF_1 and HF_2 systems is the use of a fixed sized mould which strongly limits the possible testing conditions of the sample. In particular, it does not allow applying specific hygral and/or mechanical boundary conditions on the concrete sample. An alternative is to perform ultrasonic testing directly inside a concrete specimen of an arbitrary shape and size using embedded piezoelectric transducers. The use of embedded transducers, also called "Smart Aggregates" (SMAGs) has been initially proposed by Gu *et al.* [38] to monitor the strength of concrete using harmonic excitation, and later to monitor the state of damage using chirp excitation [39, 40]. Embedded transducers have also been used to monitor the elastic mechanical properties of concrete in [41]. At ULB-BATir, transducers based on a similar design were recently developed. Each HF_3 consists in a flat piezoelectric patch which is wrapped in a waterproof coating and embedded in a small cube or cylinder made of mortar (Figure 11). One of the advantages of this technique is that no coupling agent is needed between the sensor and the concrete. The HF_3s made at ULB-BATir have been used for the monitoring of the P-wave velocity in early age concrete [42], and to monitor the crack growth in concrete and reinforced concrete in [43, 44]. The results for early age testing are used in this paper and compared to the results obtained with the other techniques presented. We shortly recall the testing procedure which is detailed in [42].

A prismatic mould, containing a pair of HF_3s with a distance d = 56 mm is used (Figure 12). The HF_1 system is used to excite the emitter with a pulse of 800 V and 2.5 µs and record the wave at the receiver side. The testing procedure is therefore identical to the one described in Section 3.3.1, except for the fact that piezoelectric transducers of the mould are replaced by HF_3s directly embedded inside the concrete specimen.

4 RESULTS AND DISCUSSIONS

According to the results, this wide set of methods (quasi-static, resonant frequency and ultrasonic) can, finally, be divided in two groups: low frequency testing (QS_0, QS_1, QS_2, QS_3 and RF) and high frequency testing (HF_1, HF_2 and HF_3). The strain rates or loading rates, covered by these methods, are gathered in Table 3. It is worth underlining that stress amplitudes or strain amplitudes are also different from one technique to the other. Comparisons of the results obtained with these techniques are largely influenced by these parameters [45, 46].

4.1 Low frequency testing

4.1.1 *Automated quasi static loading results (QS_1 and QS_2)*

Eight tests with cyclic loadings were performed: four with BTJASPE (QS_1) and four validation tests on samples removed from the mould after the setting called QS_2. All these results are plotted in Figure 13a. For each cycle, the behaviour was sufficiently linear so that the modulus of elasticity could be calculated with a simple linear regression [20].
It can be observed (Figure 13a) that these data are fairly in good agreement, both between themselves and also when compared to classical measurements (whose stress rate was 0.50 MPa/s).
Just after t_0, from the time when the E-modulus starts to become different from a null value (6 hours) to the time when its evolution reaches a quasi-straight line (8 hours), the 4 QS_1 recordings are in a range of variation of ± 1 GPa (Figure 13b). They become more scattered after 8 hours. Considering the validation tests (QS_2), as soon as the data are available, this range presents the same type of scattering. Despite this scattering, from one batch to the other, the global response of such a protocol is quite satisfying. Indeed, the series of eight tests led to a coefficient of variation of E-modulus not greater than 13 % over a period ranging from the setting of the concrete to 48 hours. If a single concrete setting time has to be defined, from QS_1 results, a value between 6 and 8 hours can be adopted depending on a chosen definition. In our case, this definition could be the time when the data start to increase at 6 hours. In real time this point is ambiguous. Indeed, one cannot decide if this value is included in the noise of the measurements. The beginning of the quasi linear part of the recordings, at 8 hours, is totally unambiguous but, may be, a little late. A definition of a point situated between the two times could suit our problem. Indeed, such a point is clearly outside the noise and it is very close to the intersection of the extrapolated linear part with the x axis. This extrapolation could be used even if no data are available before this point.

4.1.2 *TSTM results (QS_3)*

Three samples have been cyclically loaded according to the protocol described in Section 3.1.4. In this protocol, 20 % of the compressive strength is reached in 10 seconds. This means that a constant stress rate is applied at each cycle but, as the strength is evolving continuously, this stress rate is increasing with the age of the sample. The range covered goes from 0.002 to 0.50 MPa/s over the first four days. On this period, and based on the results reported in Figure 14, a very good agreement, between the E-modulus evolutions for one sample in the QS_3 device and the model of the classical tests, can be observed, despite the fact that stress rates are not strictly similar. As a consequence, it can be inferred that the influence of the stress rate on the evolution of the E-modulus is low as it was observed for QS_1 results.

4.1.3 EMM-ARM results (RF)

The resonant frequency evolutions for the three composite beams (concrete-filled moulds), resulting from processing the recordings of the accelerometers are shown in Figure 15a. All the data of EMM-ARM (RF) is plotted according to the equivalent age, normalized to 20 ºC. By observation of Figure 15a, it is clear that all composite beams endured a significant frequency shift ranging between 27.49 Hz in the beam RF_M and 109.12 Hz in the beam RF_P. However, the differences in the resonant frequency shift in the beams reveal that the three experimental setups have quite different sensitivities. To better illustrate such added sensitivity, parametric analyses with the equations of motion of both composite beams were made, as to infer the changes in resonant frequency (dF) that occur per each GPa of increase in E-modulus of the tested concrete (dE), along the process of hardening of concrete. The results of such parametric analyses for all test setups is shown in Figure 15b, where three main conclusions can be drawn: (i) the sensitivity of all experimental setups decreases with the increase in concrete E-modulus; (ii) the frequency sensitivity of the PVC mould (RF_P) setup to changes in concrete E-modulus is markedly during the all hardening process; (*iii*) the metallic beam (RF_M) is the one that has the lower sensitivity to changes in the E-modulus of the material inside the mould despite being almost constant. This point indicates that the results should be more accurate in the beam RF_P when compared to the other beams.
The overall results of E-modulus measured by the three EMM-ARM composite beams and the reference curve of classical tests are shown in Figure 16. It is evident that the coherence of the four methods is very good at most ages of testing, once more confirming the feasibility and robustness of RF. It is however remarked that the E-modulus obtained from the metallic mould test is always slightly higher than the E-modulus obtained from the other beams (acrylic and PVC). This may be partially explained by some uncertainties in the geometry of the metallic beam due to its high local deformability (1 mm thick plates) that resulted in some local warping due to previous uses of the mould. A slight under-estimation of the final E-modulus value of RF methods in regard to the model can also be observed in Figure 16.

4.1.4 Comparison between low frequency testing method

All low frequency testing results are shown in Figure 17. For these testing methods, the standard deviations are plotted in dashed lines. The beginning of the increase of the E-modulus seems to well correspond to the final setting as explained in section 4.1.2 whatever the testing method. Between the setting and 48 hours, the kinetic of the E-modulus looks very similar whatever the testing method whereas a limited scattering is observable between the results, especially at very early age. It appears that the difference of protocol of loading (strain rate, stress amplitude) and the type of testing method did not induce any strong effect on the kinetic and the amplitude of the E-modulus. All low frequency testing method have a very good correspondence with classical extensometry results.

4.1.5 Effect of the stress amplitude and stress-rate on low frequency testing method

The variation of E-modulus as measured by these different methods is attributed to their variable strain rates and amplitude of loading. In order to quantify these effects the study of these two parameters, two types of additional tests are performed with the TSTM device at ULB. First, the effect of loading amplitude is studied. A cyclic test started a few hours after the setting. Then, every hour, a load up to 5, 10, 20 or 40 % of the compressive strength is applied to the sample within 10 s. Secondly, a similar test was performed with constant load amplitude up to 20 % of the compressive strength. In this second test, the loads were applied within 5, 10, 30 or 300 s.
The E-modulus values corresponding to the variable stress/strength ratio are displayed in figure 18 a. It is observed that with the increase of the applied stress, the estimated E-modulus decreases, and this effect progressively diminishes as the concrete hardens. On Figure 18 b, this amplitude effect is quantified. Each point is obtained by linear interpolation of the experimental results. For any given loading age, a non-linear relationship is observed between the loading amplitude and the E-modulus. This confirms that the stress-strain relationship is in fact non-linear, and can be described by a quadratic equation [46] such as equation 6, where *m* is the non-linear parameter. This expression is not based on any mechanical concept but it is the result of a mathematical fitting on basis of the experimental results. As it was shown in [46], the non-linear parameter *m* in the stress-strain relationship is dependent on the concrete mix design and the degree of hydration. As concrete hardens and the E-modulus increases, the slope of this stress-strain relationship decreases.

$$\sigma = E \cdot \varepsilon - m \cdot \varepsilon^2 \tag{6}$$

The dependency of E to the stress/strength ratio is described in equation 7, where σ is the applied stress, f_{cm} is the compressive strength, E_{ref} is the elastic modulus corresponding to a reference stress/strength ratio of 20 % applied in 10 s, and A is a time-dependent amplitude parameter describing the effect of a variation of stress on the apparent measurement of E.

$$E\left(t, \frac{\sigma}{f_{cm}}\right) = E_{ref}(t) + A(t) \cdot \left(\frac{\sigma(t)}{f_{cm}(t)} - 0.2\right) \tag{7}$$

Where $E(t, \sigma/f_{cm})$, $E_{ref}(t)$ and $A(t)$ are expressed in GPa,
t: equivalent time since mixing (in hours),
$\sigma(t)$, $f_{cm}(t)$ are expressed in MPa.

The evolution of parameters E_{ref} and A are shown in Figure 20 a. The evolution of A confirms that the decrease of E due to an increase of the loading amplitude is especially strong at very early age, and drops to low values during hardening. The expression of A is provided in equation 8.

$$A(t) = A_1 \cdot \left(\frac{t}{\tau}\right)^{A_2} \tag{8}$$

Where A_1= -128 GPa, A_2=-1.015 and $\boldsymbol{\tau}$=1 h.

A second test was performed at various loading durations ($t_{loading}$) of 5, 10, 30 and 300 seconds for a constant load corresponding to 20 % of the compressive strength. The results presented in Figure 19 a suggest that for longer loading duration, the E-modulus decreases. For any loading age, it is observed that the E-modulus increases as a power law of $t_{loading}^{-1}$. The best-fit parameters indicate that as the E-modulus increases, the relative impact of the loading duration decreases. In other words, as hydration advances, the E-modulus is less affected by variations in the loading stress rate. This observation is due to the visco-elastic behaviour of concrete, which viscous properties decrease with hydration.

This loading stress rate effect is taken into account in equation 9, where E_{ref} represents the E-modulus corresponding to a loading duration of 10 seconds up to a stress/strength ratio of 20 %, $t_{loading}$ is the loading duration, and V is a time-dependent velocity parameter describing the effect of a variation of the loading stress rate on the apparent measurement of E.

$$E(t, t_{loading}) = E_{ref}(t) \cdot \left(\frac{10.\ \tau}{3600.\ t_{loading}}\right)^{V(t)} \tag{9}$$

The evolution of parameters E_{ref} and V are shown in Figure 20 b. The evolution of V confirms that the decrease of E due to an increase of loading stress rate is especially strong at very early age, and drops to low values during hardening. The expression of V is provided in equation 10.

$$V(t) = \frac{V_1}{\ln\left(\frac{t}{\tau}\right) + V_2} \tag{10}$$

Where $E(t, t_{loading})$and $E_{ref}(t)$ are expressed in GPa,
V_1=0.03, V_2=-1.179 and $\boldsymbol{\tau}$= 1 h.
t is expressed in equivalent time since mixing (in hours) and $t_{loading}$ is expressed in hours

Ultimately, the combined effect of loading stress rate and amplitude can be taken into account by equation 11.

$$E\left(t,\frac{\sigma}{f_{cm}},t_{loading}\right)=\left(E_{ref}(t)+A(t)\cdot\left(\frac{\sigma(t)}{f_{cm}(t)}-0.2\right)\right)\cdot\left(\frac{10.\ \tau}{t_{loading}}\right)^{V(t)} \tag{11}$$

Quasi-static testing for the determination of E-modulus is generally performed for loading durations between 1 and 300 seconds and that the loading amplitude is generally between 5 and 40 % of f_{cm}. Based on these parameters, two envelope curves can be computed, showing the upper and lower boundaries of the E-modulus based on the effect of loading stress rate and amplitude. The envelope curves are shown in Figure 21 and confronted to the experimental E-modulus results obtained by extensometry at ULB, IFSTTAR and U Minho (Figure 2). These experimental points, obtained for similar testing parameters, indicate that the error relative to the reproducibility of the test is of the same order of magnitude than the effect of loading stress rate or amplitude. As explained later on, by changing by several orders of magnitude the loading stress rate and/or amplitude (such as in the case of ultrasonic testing) these effects are much more visible.

4.2 High frequency testing (HF_1, HF_2, HF_3)

The results obtained on three batches with the FreshCon (HF_1) for the transmitted P-waves and S-waves velocity are shown in Figure 22. The P-waves velocity increases rapidly during setting and stabilizes after the final setting time to a value slightly superior to 4000 m/s. However, the S-waves hardly propagate though fluids. It is only at the beginning of the hardening that the S-waves velocity increases. Then, it slowly reaches a value close to 2500 m/s. These observations are in good agreement with the few results found in the literature [47, 48]. The results obtained on three batches with the BTPULS (HF_2) for the P-waves velocity transmission are shown in Figure 23 a.
The P-wave velocity results obtained, for the same concrete, with the SMAGs (HF_3) and the BTPULS (HF_2) systems are compared to the results obtained with the FreshCon (HF_1). Results are plotted on Figure 23 b. In this figure, the average of three samples is shown for the HF_1 and the HF_2.
HF_1 seems to give slightly different results, in the first part of the curve. However, this difference mainly occurs before t_0. More explanations about this observation are given in [49]. From 12 hours onward, the overall tendency is the same for all techniques, with similar values of P-waves velocity. Discrepancies before t_0 can be due to different air content in the different moulds. Indeed, different techniques are used for placing the concrete in the moulds. HF_3s are placed in a large steel mould. Its high weight (concrete + steel) makes the vibrating table less effective. On the other hand, the HF_1 samples are efficiently vibrated until no more air bubbles are trapped between the concrete and the sensors. Vibrating needles are used for HF_2. Indeed, it is known that a strong dependency of the early age P-waves velocity to the air content of the mix exists. In aired mixes, the initial velocity is around 250 m/s, whereas for de-aired mixes, initial values close to 1500 m/s can be observed [13, 50]. Ultimately, the coherence between the three experimental techniques and the good reproducibility of HF_1, the distance of 47 mm between sensors is enough in order to provide representative measurements.

With the HF_1 system, P-waves and S-waves were simultaneously measured on the same concrete with dedicated HF_1 containers, which allows an accurate computation of the high frequency E-modulus (E_{dyn}) and Poisson's ratio as shown on Figure 24.
In the case where no S-waves measurements is possible, taking a constant value of ν_{dyn} in the equation for the computation of E_{dyn} (equation 5) leads to substantial errors, especially at early age. Indeed, the E_{dyn} value is governed by the S-waves velocity evolution. The approximation made by considering a constant ν_{dyn} results in an overestimation of the early age high frequency modulus. However, in order to evaluate the relevance of HF_3 and HF_2 methods compared to usual UPV measurements, a constant ν_{dyn} of 0.3 has been considered as no S-wave measurements have yet been performed with these techniques. In figure 25, the values for the HF_1 mean curve with a constant ν_{dyn} equal to 0.3 and the HF_3 mean curve seem to stabilise after 30 hours, whereas the values of the HF_1 mean curve with consideration of the evolution of ν_{dyn} follows the trend of the static E-modulus given by the model with increasing values after 30 hours.
Before the setting time, a scattering is observable between all the high frequency testing methods (see Figure 25). However, the results computed from the P-wave and S-wave velocity (HF_1) exhibit the lowest amplitude because, before t_0, the values of ν_{dyn} are much higher than 0.3. After t_0, the kinetic looks similar whatever the high frequency testing method is. On the contrary for this case, the results computed from the P-wave and S-wave velocity (HF_1) exhibit the highest amplitude because, after t_0, the values of ν_{dyn} tend to lower values than 0.3 (see Figure 24). Therefore, as observed in [47], the computation of E_{dyn} only from P-wave velocity should be considered as a qualitative indicator of the E-modulus development.

4.3 Relation between quasi-static or low-frequency and high frequency measurements

Since the 1970s, high frequency determination of the elastic modulus began to be performed on concrete due to obvious advantages of non-destructive and continuous aspects of this method [51, 52, 53]. Some authors found relationships linking the quasi-static or low-frequency elastic modulus to the high frequency elastic modulus (Table 5) of hardened concretes.

These empirical equations illustrate the fact that high frequency values are always higher than low-frequency values of elastic modulus, which is generally true for all viscoelastic materials. This observation was confirmed experimentally at early age by several authors as well as in this study [54, 55, 56]. However, in this research, these three relations do not seem to apply, especially at very early age. Two main drawbacks to these equations are advanced here. First, the lack of physical meaning to p and q in the general equation: $E_{LF} = p \cdot E_{HF} - q$ which does not allow to take into account different concrete compositions (w/c, paste volume, cement type). Secondly, as shown in this study, the "low-frequency" or "high frequency" value can be dependent on the measuring method. Depending on the strain rate or loading amplitude for the low-frequency and high frequency measurements, different values of E_{HF} and E_{LF} can be obtained [46]. Therefore, the relationship between both values is ambiguous and certainly not intrinsic for a given concrete. In summary, the p and q parameters are dependent on the concrete composition, on the measurement method of low-frequency and high frequency modulus and, certainly, on the hydration degree. However, based on the hypothesis that the main parameters affecting the difference between E_{HF} and E_{LF} are the loading stress rate and amplitude, such a linear relationship between both properties is consistent with the modelling approach of equation 11.

In the case of a given experimental protocol to determine E_{HF} and E_{LF} on a given concrete, an equation of the type $E_{LF} = p \cdot(E_{HF} - q)$ (with $p > 1$ and $q > 0$) seems appropriate to describe the behaviour of concrete throughout the hardening process. Indeed, at the initial setting time, the low-frequency modulus is close to 0. However, due to the initial increase of the ultrasonic pulse velocity before that time, the high frequency modulus has already reached a significant value. The q parameter represents this initial gap. Then, as concrete hardens, E_{LF} tends to increase whereas E_{HF} stabilizes more rapidly. Therefore, the gap between low-frequency and high frequency values tends to decrease throughout hydration, thus explaining the p parameter, which is representative of the different kinetics of the low-frequency and high frequency modulus evolution.

Figure 26 shows this relationship in this case by comparison of the HF_1 results and the classical extensometry results between the setting time and 66 hours. No linearity between E_{HF} and E_{LF} is directly observable here. But if only results after 18 hours (E_{LF} = 16 GPa) are considered, a linear relationship is observable. Then, it appears that the relationship between E_{HF} and E_{LF} cannot be assumed as fully linear. Here, this assumption is only available between 18 and 66 hours. Further research should be carried out in order to be able to determine with precision the loading stress rate and amplitude of the high frequency measurements. Such measurement could improve the model presented in equation 11, and confirm the hypothesis that through the mechanism of very short term creep, the loading stress rate and amplitude are indeed the main parameters affecting the apparent value of the E-modulus.

Finally Figure 27 presents the synthesis of all results. Only mean values of each testing method are shown here. As expected, clear differences appear between low-frequency and high frequency results. High frequency modulus values with consideration of the evolution of ν_{HF} are always higher than low-frequency results. A faster evolution of high frequency results is also observable.

5 CONCLUSIONS

Different automatic techniques aimed at measuring changes in the stiffness of a concrete at early age were used in three different laboratories. They were grouped in low-frequency and high frequency methods.

The low-frequency methods gave responses similar to classical measurements. These classical measurements consist in performing the test after having removed the samples from their mould just after the setting time. Despite the fact that the samples are very brittle, the concrete begins to harden at the end of the working day thus, automatic methods are almost obligatory to study this initial phase of concrete behaviour. Two of the low-frequency methods are based on the use of laboratory testing machine (TSTM or QS_3, BTJASPE or QS_1) whereas the third method (EMM-ARM or RF) is well adapted for laboratory testing and in field. Their mutual performances are in good agreement. For such inter-laboratories tests, the protocols of mixing and loading should be improved, though.

Both the loading stress rate and amplitude are observed to have an effect on the determination of the low-frequency elastic modulus. This observation, which might be explained by very short term creep, is of limited importance when quasi-static measurements are performed, regarding the reproducibility of such tests. However, similar mechanisms could explain the difference between the low-frequency and high frequency elastic modulus, since both are measured at very different loading rate and amplitudes.

The ultrasonic measurements are also automatic methods and they are good candidates for the monitoring of the stiffness of the concrete at very early age. Two classical techniques (FreshCon or HF_1, BTPULS or HF_2) are compared to a newly developed technique (SMAGs or HF_3). Ultrasonic measurements provide values of E-

modulus that are higher than the values provided by the quasi static or low frequency tests at the time of the concrete setting. This difference decreases as the concrete hardens. Their results show a clear effect of the loading rate on the E-modulus calculation compared to values obtained with quasi static tests. A correlation between the results of high frequency techniques and low frequency ones is not yet clearly accessible and models should be found to promote the use of ultrasonic techniques applied to the monitoring of the concrete stiffness at very early age.
Further experimentations are needed to quantify accurately the effect of the strain or stress rates on the evolution of the elastic modulus in the low frequency and high frequency ranges.

6 ACKNOWLEDGEMENTS

These researches were performed thanks to the "Hubert Curien" Partnerships passed, on one hand, between IFSTTAR & ULB (Tournesol project) and, on the other hand, between IFSTTAR & the University of Minho (Pessoa project – Proc 441, together with the Portuguese Foundation for Science and Technology - FCT). A special thank is addressed to the Campus France agency (http://www.campusfrance.org) for their management of these partnerships. The authors are also grateful to the financial support provided by FCT (Portuguese Foundation for Science and Technology) through PhD grant (SFRH / BD / 80682 / 2011) to the third author and the research project EXPL/ECM-EST/1323/2013. The second, fourth and last four authors would like to thank the Belgian national founds for scientific research (FNRS) for their financial support to the Université Libre de Bruxelles.

7 REFERENCES

[01] Acker P. and Michaud-Poupardin V. (2002) Limiting cracking: Essential conditions for ensuring the durability of concrete structures. Bulletin des Laboratoires des Ponts et Chaussées, 238, May-June, ref. 4433, 13-25.
[02] ACI (1999) Manual of Concrete Practice. Part 2. Construction practices and inspection pavements. ACI 305R-91.
[03] Aïtcin P.C. (1998) Autogenous shrinkage measurement, Autoshrink 98. Proc. International Workshop on Autogenous Shrinkage of Concrete. E. Tazawa (Ed), Hiroshima, Japan, 245-256.
[04] Weiss W. J. (2002) Experimental determination of the 'Time Zero', t0 ('Maturity-Zero', M0). Early Age Cracking in Cementitious Systems - Report of RILEM Technical Committee 181-EAS - Early age shrinkage induced stresses and cracking in cementitious systems. A. Bentur (Ed), Ch. 6.1, 195-206.
[05] Sant G., Dehadrai M., Bentz D., Lura P., Ferraris C.F., Bullard J.W. and Weiss J. (2009) Detecting the fluid to solid transition in cement pastes. *Concrete International* **31**: 53-58.
[06] Boulay C., Staquet S., Azenha M., Deraemaeker A., Crespini M., Delsaute B., Granja J., Carette J., Dumoulin C., Karaiskos G. (2013) Monitoring elastic properties of concrete since early age by means of cyclic loadings, ultrasonic measurements, natural resonant frequency of a composite beam (EMM-ARM) and with smart aggregates. Proc. 8^{th} International Conference on Fracture Mechanics of Concrete and Concrete Structures FraMCoS-8, March 10^{th} – 14^{th}, Toledo, Spain, 185.
[07] Carino N. and Lew H. (2001) The maturity method: from theory to application. Proc. of the 2001 Structures Congres & Exposition, 1-19.
[08] Rastrup E. (1954) Heat of hydration in concrete. *Magazine of concrete research* **6**: 79-92.
[09] Mc Intosh J.D. (1956) Effect of low temperature curing on the compressive strength of concrete. Proc. RILEM symposium on winter concreting, Danish institute for building research, Copenhagen, Session B II, 3-17.
[10] D'Aloïa L. (2003) Early age kinetics activation energy, maturity and equivalent age. Report of the RILEM TC181- Early age shrinkage induced stresses and cracking in cementitious systems, report 25, chap. 4.6, 127-148.
[11] C403/C403M-08 Standard Test Method for Time of Setting of Concrete Mixtures by Penetration Resistance
[12] EN 480-2:2006. Admixtures for concrete, mortar and grout. Determination of setting time.
[13] Robeyst N., Gruyaert E., Grosse C.U., De Belie N. (2008) Monitoring the setting of concrete containing blast-furnace slag by measuring the ultrasonic p-wave velocity. *Cement and Concrete Research* **38**: 1169–1176.
[14] Bentur A. (2003) Early Age Cracking in Cementitious Systems. *RILEM Report 25*, 13-15.
[15] Morgan P.H., Mercer L.P. and Flodin N.W. (1975) General model for nutritional responses of higher organisms. Proc. National Academy of Sciences of the United States of America, 4327-4331.
[16] Boulay C. and Colson A., (1979) Un extensomètre à béton éliminant l'influence des déformations transversales sur la mesure des déformations longitudinales. *Materials and Structures* **14:** 35-38.
[17] Torrenti J.M., Dantec P., Boulay C. and Semblat J.F. (1999) Projet de processus d'essai pour la détermination du module de déformation longitudinale du béton. Bulletin de Liaison des Ponts et Chaussées, # 220, March April, 79-81.
[18] LNEC (1993). Betões - Determinação do módulo de elasticidade em compressão. E 397.

[19] Boulay C., Merliot E., Staquet S. and Marzouk O. (2010) Monitoring of the concrete setting with an automatic method. Proc. 13th International Conference and Exhibition: Structural Faults and Repair, Edinburgh, UK, June 15th – 17th.

[20] Boulay C., Staquet S., Delsaute B., Carette J., Crespini M., Yazoghli-Marzouk O., Merliot E. and Ramanich S. (2014) How to monitor the modulus of elasticity of concrete, automatically since the earliest age? *Materials and Structures* **47**: 141-155.

[21] Boulay C., Crespini M., Delsaute B. and Staquet S. (2012) Monitoring of the creep and the relaxation behaviour of concrete since setting time, part 1: compression. Proc. SSCS 2012 (Numerical Modeling – Strategies for Sustainable Concrete Structures), Aix en Provence, France, May 29th – June 1st, 1-10.

[22] Boulay C., Crespini M., Carette J. and Staquet S. (2012) Elastic properties of concrete at early age: monitoring of the E-modulus and the Poisson's ratio with cyclic loadings and ultrasonic measurements. Proc. 14th International Conference Structural Faults and repair-2012, July 3rd – 5th, Edinburgh, UK, 1-11.

[23] Staquet S., Delsaute B., Darquennes A. and Espion B. (2012) Design of a revisited TSTM sys-tem for testing concrete since setting time under free and restraint conditions. Proc. Concrack3 – Rilem-JCI International Workshop on Crack Control of Mass Concrete and Related Issues Concerning Early-age of concrete structures, March 15th – 16th, Paris, France, 99-110.

[24] Delsaute B., Staquet S. and Boulay C. (2012) Monitoring of the creep and the relaxation behaviour of concrete since setting time, part 2: tension. Proc. SSCS 2012 (Numerical Modeling – Strategies for Sustainable Concrete Structures), Aix en Provence, France, May 29th – June 1st, 1-10.

[25] Azenha M., Magalhães F., Faria R. and Cunha Á. (2010) Measurement of concrete E-modulus evolution since casting: A novel method based on ambient vibration. *Cement and Concrete Research* **40**: 1096-105.

[26] Azenha M., Faria R., Magalhaes F., Ramos L. and Cunha A. (2012) Measurement of the E-modulus of cement pastes and mortars since casting, using a vibration based technique. *Materials and Structures* **45**: 81-92.

[27] Azenha M., Ferreira C., Silva J., Correia A.G., Aguilar R. and Ramos L.F. (2011) Continuous stiffness monitoring of cemented sand through resonant frequency. Proc. Emerging Technologies for Material, Design, Rehabilitation, and Inspection of Roadway Pavements, Hunan, China, 174-183.

[28] Granja J.L., Fernandes P., Benedetti A., Azenha M. and Sena-Cruz J. (2015) Monitoring the early stiffness development in epoxy adhesives for structural strengthening. *International Journal of Adhesion and Adhesives* **59**: 77-85.

[29] Azenha M., Ramos L.F., Aguilar R. and Granja J.L. (2012) Continuous monitoring of concrete E-modulus since casting based on modal identification: A case study for in situ application. *Cement and Concrete Composites* **34**: 881-890.

[30] Welch P.D. (1967) The use of Fast Fourier Transform for the Estimation of Power Spectra: a method based on time averageing over short, modified periodograms. *IEEE Transactions on Audio and Electroacoustics* **15**: 70-73.

[31] NI (2010) LabVIEW. Ed National Instruments.

[32] Karaiskos G., Deraemaeker A., Aggelis D.G. and Van Hemelrijck D. (2015) Monitoring of concrete structures using the ultrasonic pulse velocity method. *Smart Materials and Structures* (accepted for publication).

[33] Reinhardt H.W. and Grosse C.U. (2004) Continuous Monitoring of setting and hardening of mortar and concrete. *Construction and Building Materials* **18**: 145-154.

[34] Krüger M., Grosse C.U. and Lehmann F. (2013) Automated Shear-Wave Techniques to Investigate the Setting and Hardening of Concrete in Through-Transmission. In: Nondestructive Testing of Materials and Structures, O. Güneş and Y. Akkaya (Eds). Springer Netherlands: 431-436.

[35] Staquet S., Boulay C., Robeyst N. and De Belie N. (2008) Ultrasonic monitoring of setting and autogenous shrinkage development of high performance concrete. Proc. 8th International Conference on Creep, Shrinkage and Durability of Concrete and Concrete Structures (CONCREEP 8), 321-327.

[36] Zhu J., Kee S.-H., Han D. and Tsai Y.-T. (2011) Effects of air voids on ultrasonic wave propagation in early age cement pastes. *Cement and Concrete Research* **41**: 872-881.

[37] Cannard G., Orcel G. and Prost J. (1990) Le suivi de la prise des ciments par ultrasons. Bulletin de liaison des laboratoires des Ponts et Chaussées, n° 168, 89–95.

[38] Gu H., Song G., Dhonde H., Mo Y.L. and Yan S. (2006) Concrete early-age strength monitoring using embedded piezoelectric transducers. *Smart Materials and Structures* **15**: 1837-1845.

[39] Song G., Gu H. and Mo Y.-L. (2008) Smart aggregates: multi-functional sensors for concrete structures - a tutorial and a review. *Smart Materials and Structures* **17**: 033001.

[40] Song G., Gu H., Mo Y.L., Hsu T.T.C. and Dhonde H. (2007) Concrete structural health monitoring using embedded piezoceramic transducers. *Smart Materials and Structures* **16**: 959.

[41] Li Z., Qin L. and Huang S. (2009) Embedded Piezo-Transducer in Concrete for Property Diagnosis. *Journal of Materials in Civil Engineering* **21**: 643-647.

[42] Dumoulin C., Karaiskos G., Carette J., Staquet S. and Deraemaeker A. (2012) Monitoring of the ultrasonic P-wave velocity in early-age concrete with embedded piezoelectric transducers. *Smart Materials and Structures*, **21**: 047001.
[43] Dumoulin C., Karaiskos G., Sener J.Y. and Deraemaeker A. (2014) Online monitoring of cracking in concrete structures using embedded piezoelectric transducers. *Smart Materials and Structures* **23**: 115016.
[44] Karaiskos G., Flawinne S., Sener J.-Y. and Deraemaeker A. (2013) Design and validation of embedded piezoelectric transducers for damage detection applications in concrete structures. Proc. 10th International Conference on Damage Assessment of Structures (DAMAS 2013), Dublin, Ireland.
[45] Han S.-H. and Kim J.-K. (2004) Effect of temperature and age on the relationship between dynamic and static elastic modulus of concrete. *Cement and Concrete Research* **34**: 1219-1227.
[46] Shkolnik I.E. (2005) Effect of nonlinear response of concrete on its elastic modulus and strength. *Cement and Concrete Composites* **27**: 747-757.
[47] Van Den Abeele K., Desadeleer W., De Schutter G. and Wevers M. (2009) Active and passive monitoring of the early hydration process in concrete using linear and nonlinear acoustics. *Cement and Concrete Research* **39**: 426-432.
[48] Benmeddour F., Villain G., Abraham O. and Choinska M. (2012) Development of an ultrasonic experimental device to characterise concrete for structural repair. *Construction and Building Materials* **37**: 934-942.
[49] Carette J., Dumoulin C., Karaiskos G., Staquet S. and Deraemaeker A. (2012) Monitoring of the E-modulus in early age concrete since setting time with embedded piezoelectric transducers. Proc. Conference: Structural Faults & Repair, 14th International Conference and Exhibition, Edinburgh, Scotland, UK, 1-7.
[50] Zhu J., Kee S.-H., Han D. and Tsai Y.-T. (2011) Effects of air voids on ultrasonic wave propagation in early age cement pastes. *Cement and Concrete Research* **41**: 872-881.
[51] Lydon F.D. and Balendran R.V. (1986) Some observations on elastic properties of plain concrete. *Cement and Concrete Research* **16**: 314-324.
[52] Neville A.M. and Brooks J.J. (1987) *Concrete technology*. New York: Longman Scientific & Technical.
[53] Yuan D., Nazarian S. and Zhang D. (2003) Use of stress wave techniques to monitor and predict concrete strength development. Proc. International Symposium Non-Destructive Testing in Civil Engineering (NDT-CE), 409-423.
[54] Krauß M. and Hariri K. (2006) Determination of initial degree of hydration for improvement of early-age properties of concrete using ultrasonic wave propagation. *Cement and Concrete Composites* **28**: 299-306.
[55] YildIrIm H. and Sengul O. (2011) Modulus of elasticity of substandard and normal concretes. *Construction and Building Materials* **25**: 1645-1652.
[56] Wen-bin S. and Cheng-qing W. (2009) Analytical Solutions to Strain Rates of Reinforced Concrete Simply Supported Slabs under Blast Loads. *Journal of Southwest Jiaotong University* **17**: 212-217.

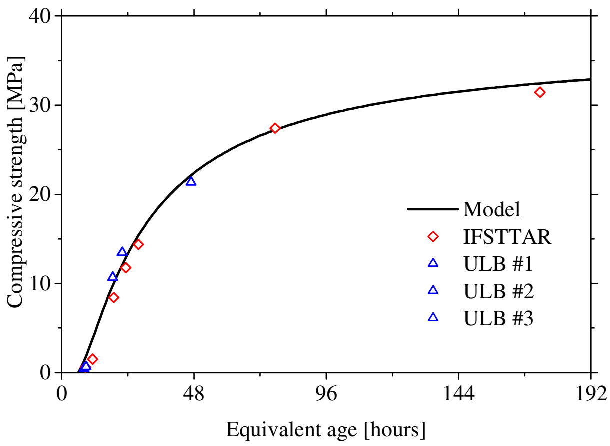

Figure 1: Compressive strength results obtained by the teams of IFSTTAR and ULB.

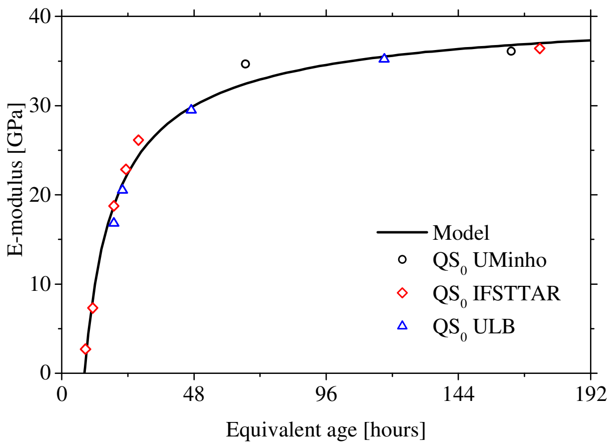

Figure 2: Evolution of the quasi-static E-modulus obtained with classical methods (QS_0). A model for quasi-static E-modulus is calibrated on these data.

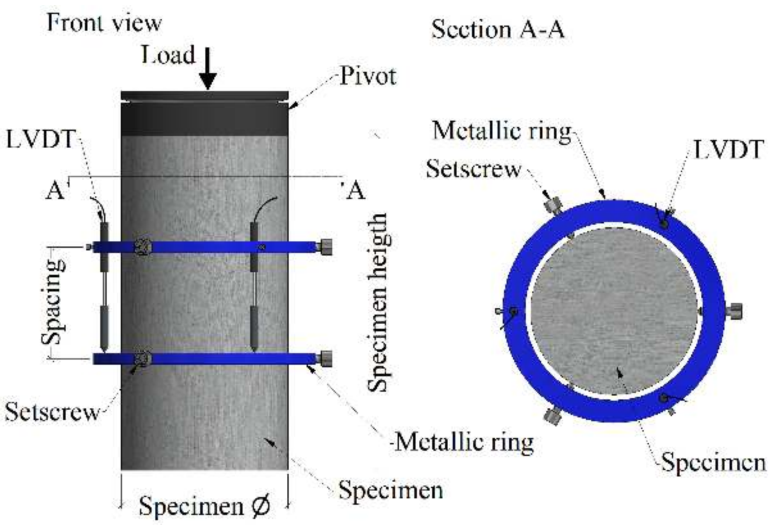

Figure 3: Classical test setup (QS_0) with extensometers for quasi static loadings on concrete cylinder for quasi-static E-modulus monitoring.

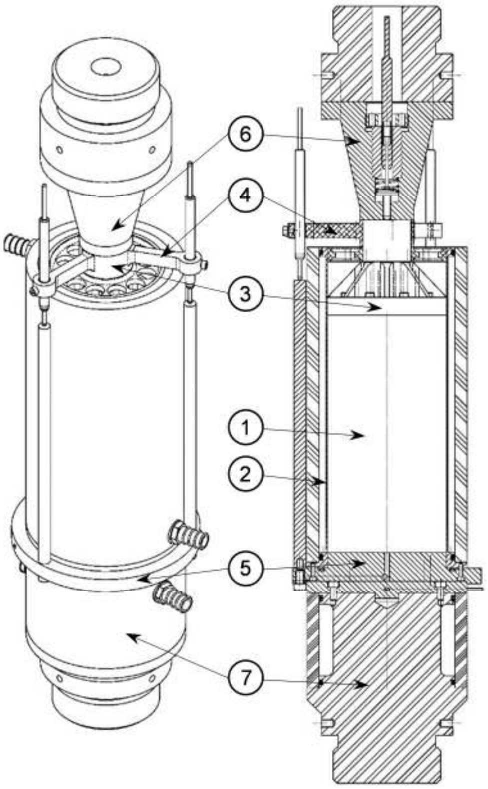

Figure 4: Test setup (QS_1) for cyclic loadings (BTJASPE) for quasi-static E-modulus monitoring.

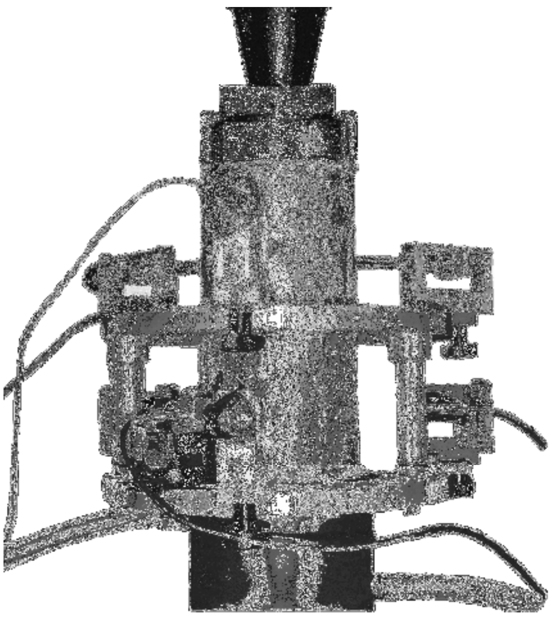

Figure 5: Validation test (QS_2) for results obtained with BTJASPE (QS_1) for quasi-static E-modulus monitoring.

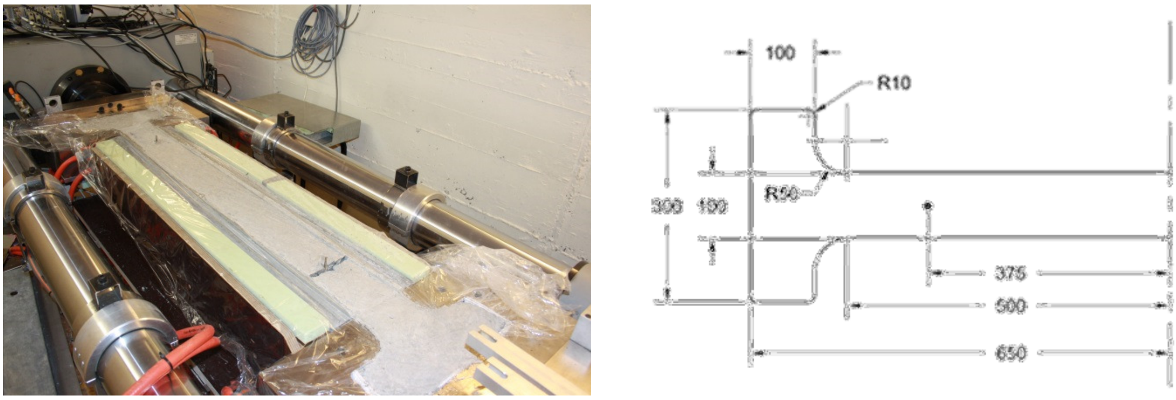

a) **b)**

Figure 6: TSTM (QS_3) equipment for cyclic loadings for quasi-static E-modulus monitoring: a) Photo; b) Dimension of the specimen (units: mm).

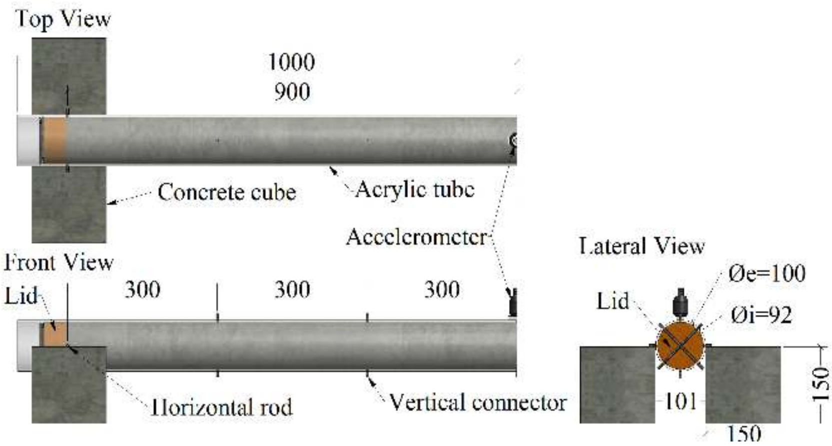

Figure 7: EMM-ARM testing with acrylic mould (RF_A) for quasi-static E-modulus monitoring (units: mm).

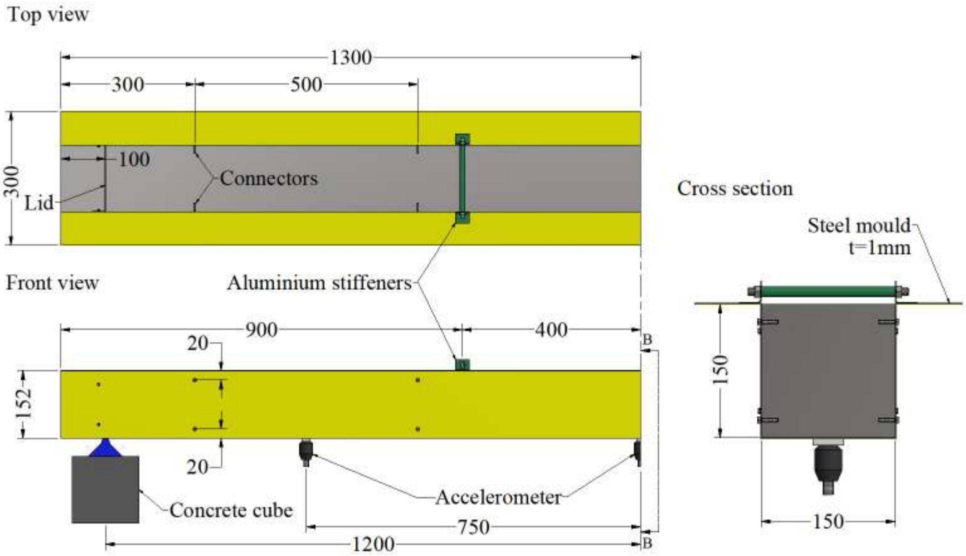

Figure 8: EMM-ARM testing with metallic mould (RF_M) for quasi-static E-modulus monitoring (units: mm).

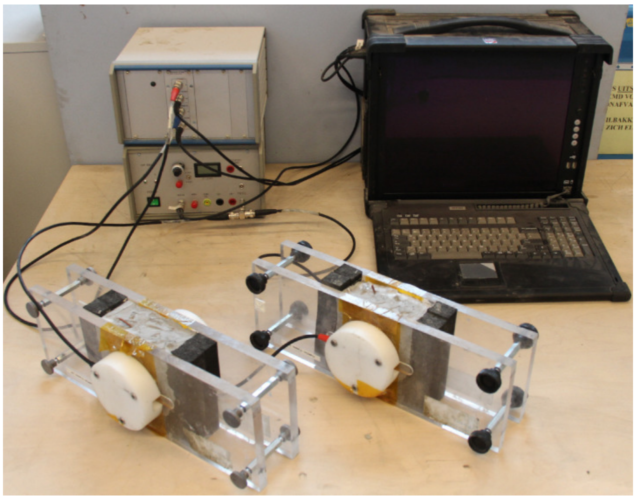

Figure 9: FreshCon System (HF_1) for high frequency E-modulus monitoring.

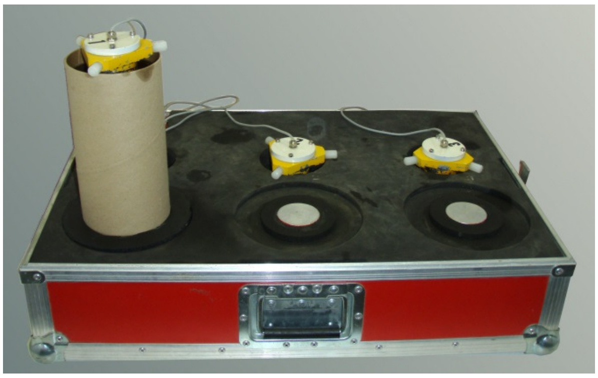

Figure 10: BTPULS system (HF_2) for high frequency E-modulus monitoring.

a) Piezoeletric patch

b) With waterproof coating

c) With conductive paint

d) Smart Aggregate

Figure 11: SMAGs sensors (HF_3) for high frequency E-modulus monitoring.

Figure 12: Prismatic mould with SMAGs before casting the concrete.

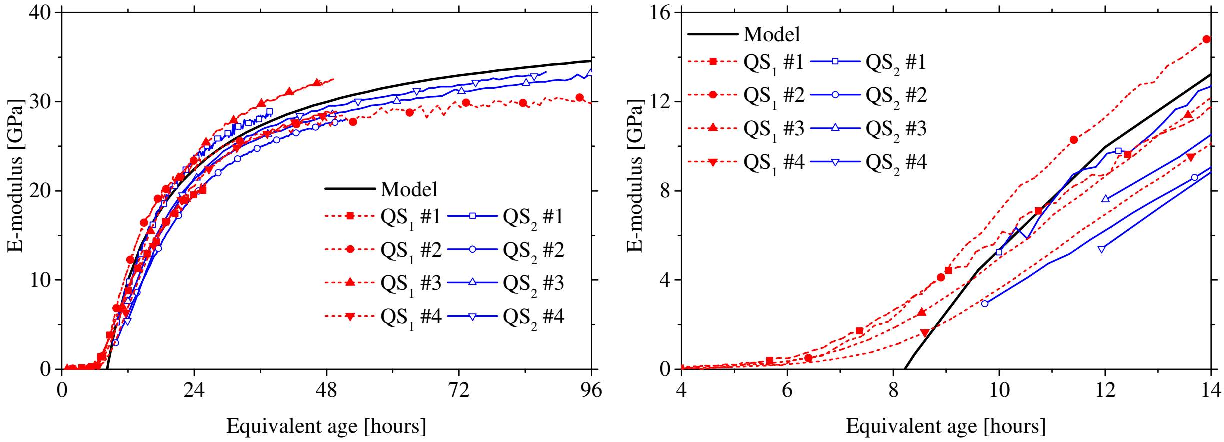

a) **b)**

Figure 13: a) Determination of the quasi-static E-modulus with BTJASPE (QS_1) and cyclic loadings on unconfined specimens (QS_2) compared to calibrated model for quasi-static E-modulus; b) Detail of the beginning of the recordings during the concrete setting.

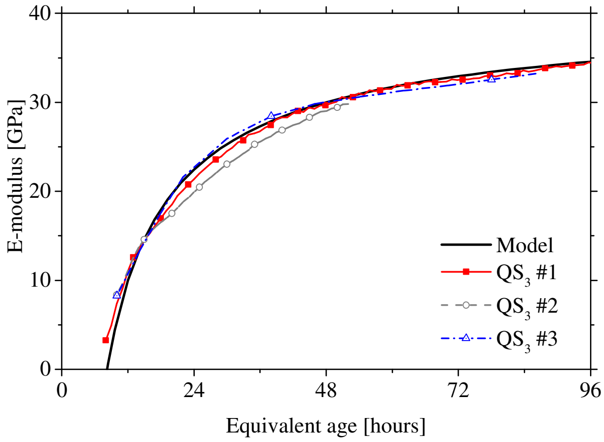

Figure 14: Quasi-static E-modulus with TSTM (QS_3) compared to calibrated model for quasi-static E-modulus.

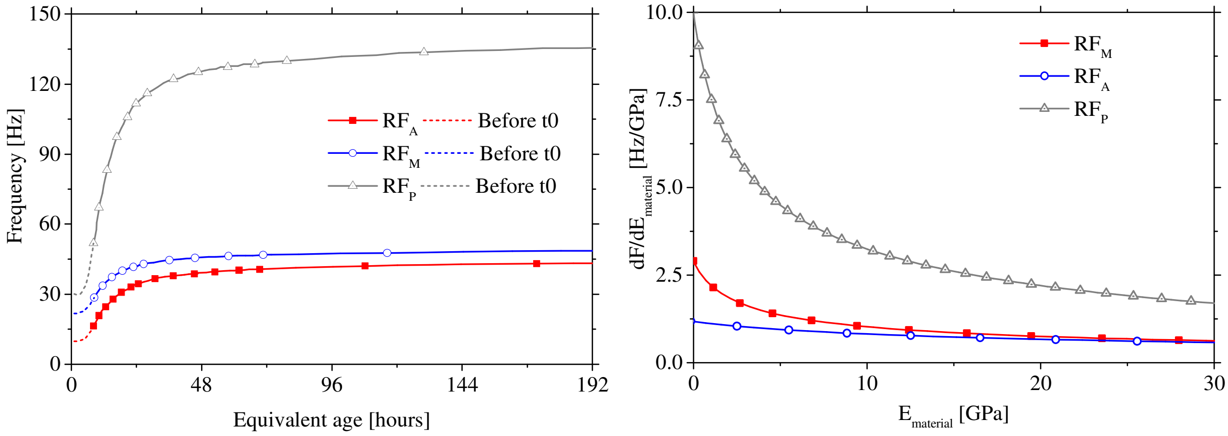

a) **b)**

Figure 15: a) Resonant frequency evolution for the acrylic, metallic and PVC EMM-ARM composite beams (RF_A, RF_M, RF_P); b) Frequency variation per E-modulus variation of concrete according to the type of mould and the state of hardening.

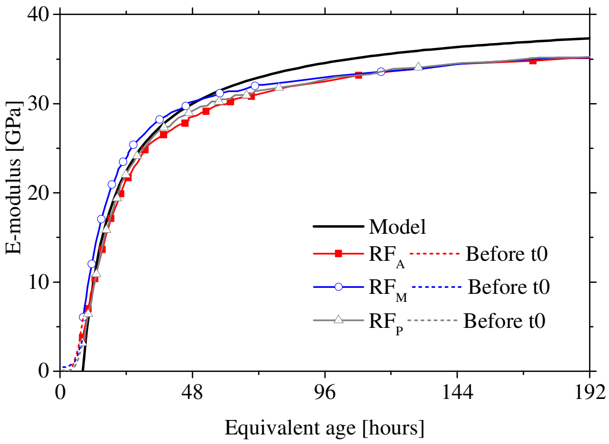

Figure 16: Quasi-static E-modulus obtained through EMM-ARM (acrylic, metallic and PVC composite beams RF_A, RF_M, RF_P) compared to calibrated model for quasi-static E-modulus.

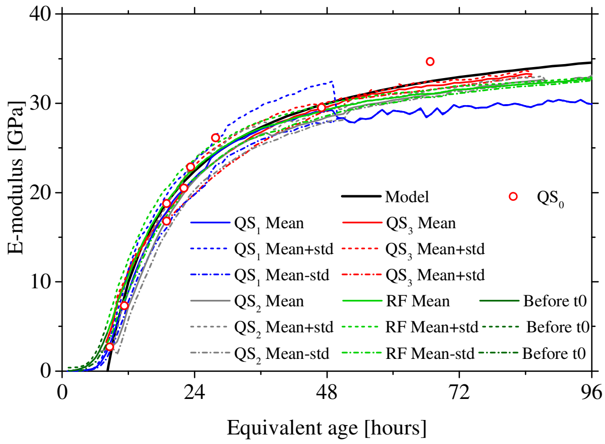

Figure 17: Quasi-static E-modulus obtained with low frequency testing methods QS_0, QS_1, QS_2, QS_3, RF compared to calibrated model for quasi-static E-modulus.

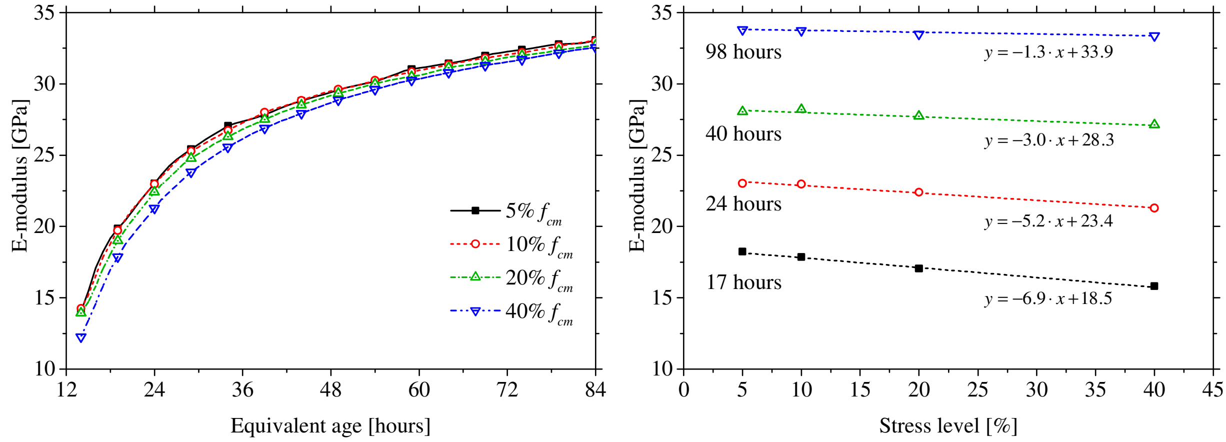

a) b)

Figure 18: a) Evolution of the E-Modulus for loading amplitudes of 5 – 10 -20 – 40% of the compressive strength; b) Evolution of the E-modulus according to the stress level for several ages of loading.

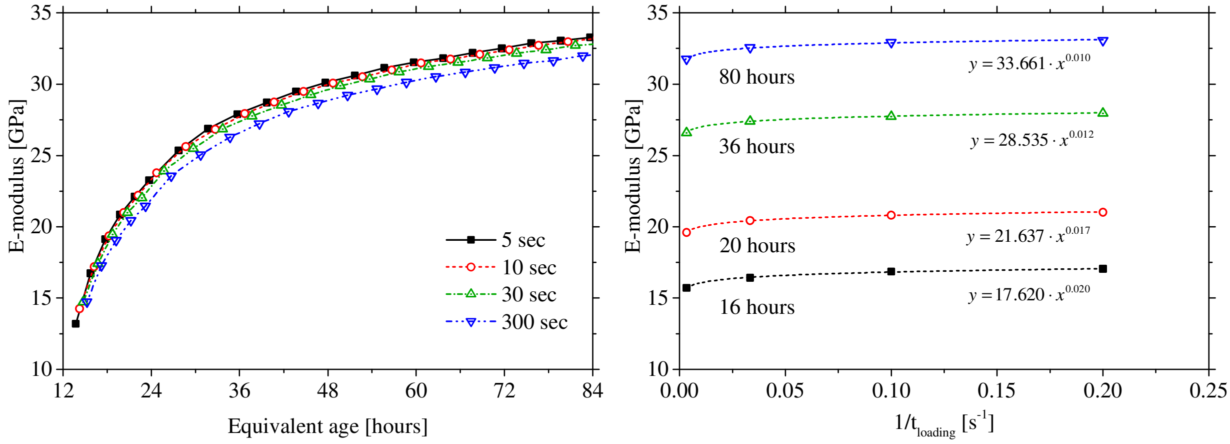

a) b)

Figure 19: a) Evolution of the E-Modulus for a stress applied in 5 – 10 – 30 or 300 seconds; b) Evolution of the E-modulus according to the velocity of loading for several ages of loading.

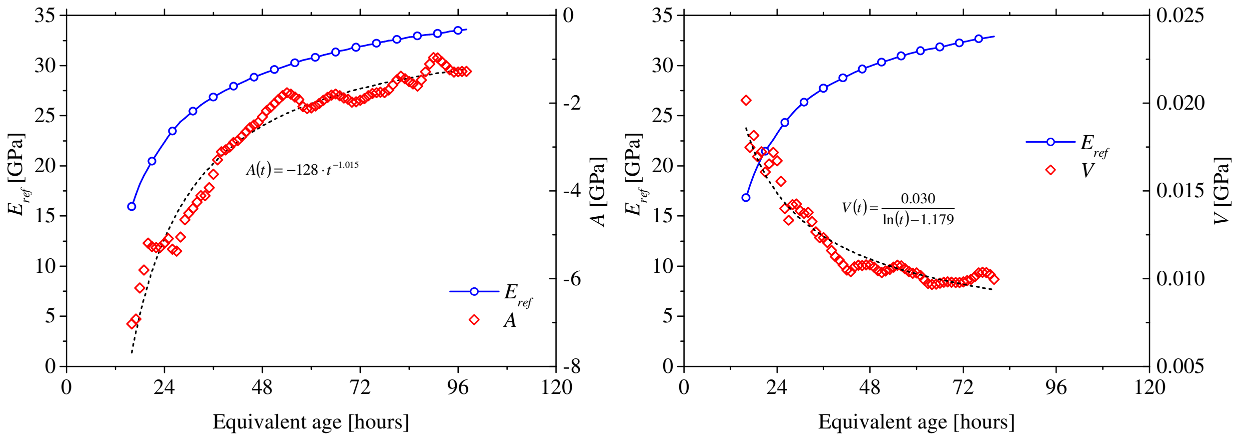

a) b)

Figure 20: a) Evolution of E_{ref} and amplitude parameter A determined with a single TSTM test (QS_3); b) evolution of E_{ref} and velocity parameter V determined with a single TSTM test (QS_3).

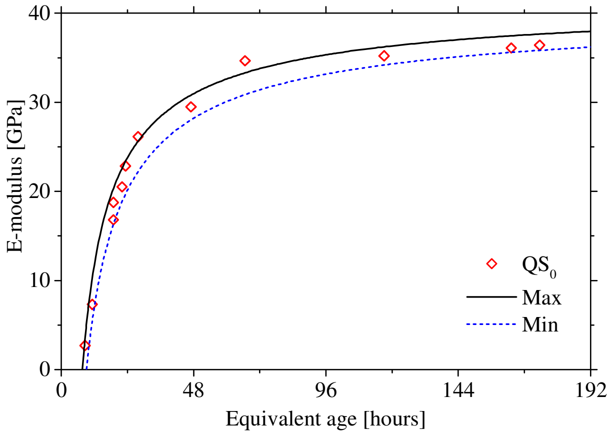

Figure 21: Lower and upper boundaries for the effect of loading stress rate and amplitude on quasi-static determination of E-modulus.

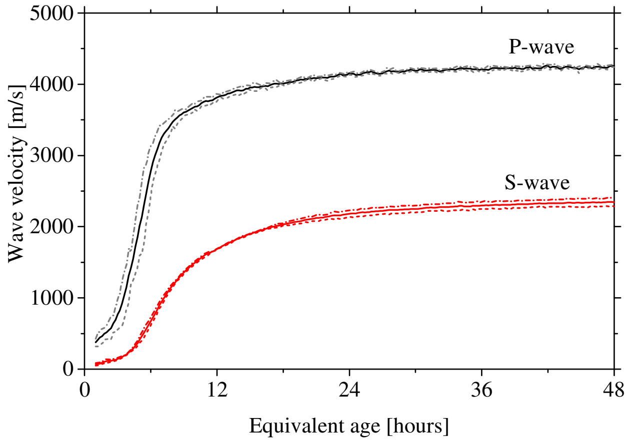

Figure 22: P-waves and S-waves velocity evolution through the FreshCon system (HF_1).

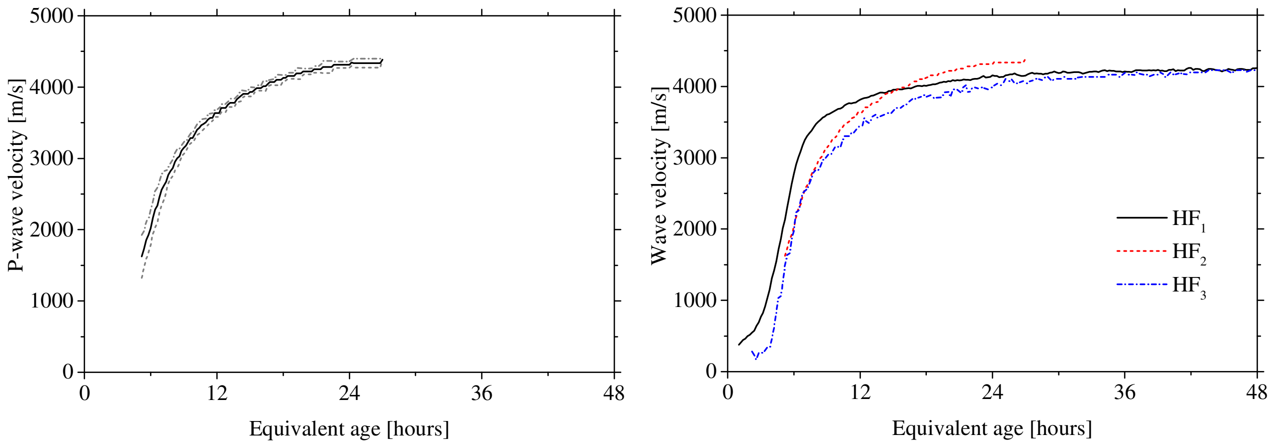

a) **b)**

Figure 23: a) Three sets of results obtained with BTPULS system (HF_2); b) Comparison of the measured P-wave velocities using FreshCon (HF_1), BTPULS (HF_2), and SMAGs (HF_3).

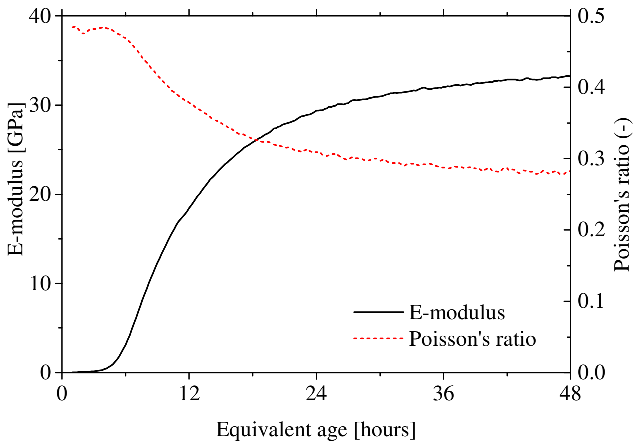

Figure 24: Evolution of high frequency E modulus and Poisson ratio computed from the P-wave and S-wave velocity with the FreshCon system (HF_1).

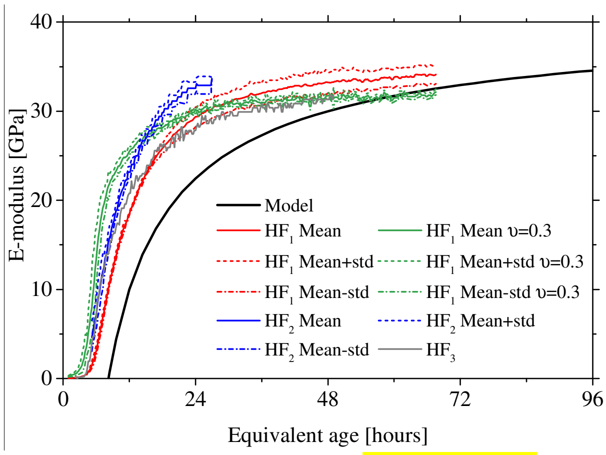

Figure 25: Comparison of the high frequency E-modulus computed from the P-wave velocity only with ν_{dyn} = 0.3 (FreshCon (HF_1), BTPULS (HF_2), SMAG (HF_3)) and from the P-wave and S-wave velocity (HF_1) with the quasi-static E-modulus calibrated model.

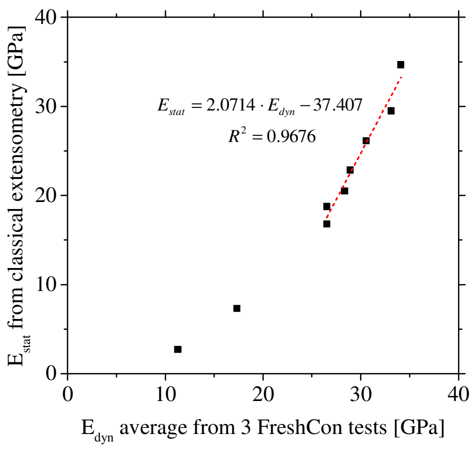

Figure 26: Relationship between high frequency E-modulus through HF_1 (from the P-wave and S-wave velocity) and modelled quasi-static E-modulus through classical extensometry with the reference test set up QS_0.

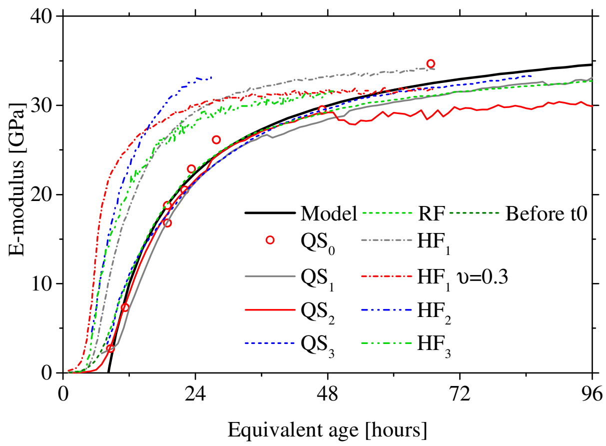

Figure 27: Comparison of E-modulus obtained with quasi-static (QS_0, QS_1, QS_2, QS_3, RF) and high frequency (HF_1, HF_2, HF_3) testing methods and with calibrated model for quasi-static E-modulus.

Table 1: Mixture proportions of the concrete, w/c: 0.54.

Components / origin	*Mass (kg /m³)*
CEM I 52.5 N PMES CP2 / Saint Vigor	340
Sand 0-4 / Bernières	739
Gravel 8-22 – Bernières	1072
Total water	184
Density of fresh concrete	2335

Table 2: Classical test setup (QS_0) in the three laboratories.

	Extensometer	*Sample*		*Protocol of loading*	
	Spacing (cm)	*Heigth (cm)*	*Diameter (cm)*	*Loading (MPa)*	*Stress rate (MPa/s)*
IFSTTAR	12	22	11	5% to 30% of f_{cm}	0.5
ULB	12	22	11	20 % of f_{cm}	0.2 to 0.55
U Minho	10	30	15	0.8 to 33% of f_{cm}	0.3

Table 3: Loading rates for each device.

Device	*Loading control (corresponding strain or stress rate)*	*Classification*
Classical tests (QS_0)	0.2 - 0.55 MPa/s	Low frequency
BTJASPE (QS_1)	5×10^{-6} /s (0.001 to 0.2 MPa/s)	
TSTM (QS_3)	10 s from 0 to 0.2 f_{cm} (0.002 to 0.5 MPa/s)	
EMM-ARM (RF)	9-45 Hz (0.1 to 1×10^{-6}/s*)	
BTPULS (HF_2)	10-100 kHz	High frequency
FreshCon (HF_1)	10-100 kHz	
Smart aggregates (HF_3)	10-100 kHz	

*Strain rate computed by double integration of recorded accelerations and use of analytical derivations [56] (beam theory).

Table 4: Classical extensometry tests (mean values) according to the reference set up QS_0.

IFSTTAR⁽¹⁾		*ULB*⁽²⁾		*U Minho*⁽³⁾	
Time (hours)	*E-modulus (GPa)*	*Time (hours)*	*E-modulus (GPa)*	*Time (hours)*	*E-modulus (GPa)*
8.64	2.72	18.96	16.8	66.72	34.66
11.28	7.32	22.08	20.5	163.2	36.1
18.96	18.76	47.04	29.5		
23.28	22.86	117.12	35.2		
27.84	26.14				
173.52	36.41				

(1) Mean values of 3 specimens
(2) Value of 1 specimen
(3) Mean values of 3 specimens

Table 5: Relations between high frequency modulus E_{HF} and quasi-static or low frequency modulus E_{LF}.

References	*Model*
Shkolnik [46]	$E_{LF} = 0.83 \cdot E_{HF}$
Van Den Abeele, *et al.* [47]	$E_{LF} = 1.25 \cdot E_{HF} - 19$
Benmeddour, *et al.* [48]	$E_{LF} = 1.033 \cdot E_{HF} - 7.245$